

Learning from Physical Human Feedback: An Object-Centric One-Shot Adaptation Method

Alvin Shek¹, Rui Chen¹, Changliu Liu¹

Abstract—For robots to be effectively deployed in novel environments and tasks, they must be able to understand the feedback expressed by humans during intervention. This can either correct undesirable behavior or indicate additional preferences. Existing methods either require repeated episodes of interactions or assume prior known reward features, which is data-inefficient and can hardly transfer to new tasks. We relax these assumptions by describing human tasks in terms of object-centric sub-tasks and interpreting physical interventions *in relation to specific objects*. Our method, Object Preference Adaptation (OPA), is composed of two key stages: 1) pre-training a base policy to produce a wide variety of behaviors, and 2) online-updating only certain weights in the model according to human feedback. The key to our fast, yet simple adaptation is that general interaction dynamics between agents and objects are fixed, and only object-specific preferences are updated. Our adaptation occurs online, requires only one human intervention (one-shot), and produces new behaviors never seen during training. Trained on cheap synthetic data instead of expensive human demonstrations, our policy demonstrates impressive adaptation to human perturbations on challenging, realistic tasks in our user study. Videos, code, and supplementary material: <https://alvinosaur.github.io/AboutMe/projects/opa>.

I. INTRODUCTION

Robots are useful in many real world tasks, e.g., where there are health risks or where tedious efforts are required. Ways to achieve desired behavior range from traditional planning and control to reinforcement or imitation learning. Cost functions, rewards, and pre-recorded demonstrations that are representative of the target scenarios are often fixed beforehand. However, during actual deployment, unpredictable factors can always arise such as varying task specifications and human preferences on how the tasks should be carried out. Such changes can be easily and naturally handled if a human can provide corrective physical feedback in real time. In such physical human-robot interactions (pHRI), robots need to understand this feedback and adapt their behavior accordingly for future tasks. In this paper, we study a special yet prevalent setting where the online human feedback is *object-centric*, as opposed to non-object-centric settings such as those encoding temporal preferences. That is, human interventions can be interpreted as leading the robot to either avoid or visit certain objects and areas in the environment with possibly preferred orientations. Hence, by leveraging this assumption, the robot can infer which objects are relevant and better understand human feedback.

Illustrating Example: To better understand this insight, consider a factory setting where a robot has been trained to

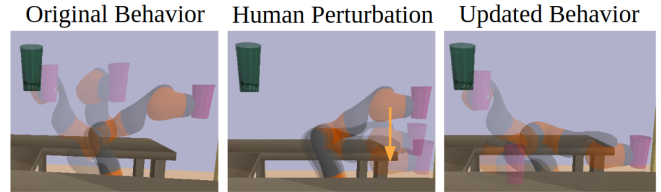


Fig. 1: OPA interprets human feedback in relation to specific objects, enabling fast online adaptation. In this scene, the default behavior (left) is to carry a cup of water straight to the hand-off location on the top left. After a downward push by the human (middle), the robot learns online to stay close to the table as it carries the cup (right).

carry printed items from a 3D printer to a bin for cleaning. Now, the manufacturing process suddenly changes: the robot should additionally place items upright in a scanner before dropping them in the cleaning bin. As a human operator, a natural and quick way to communicate this task modification would be a physical correction. After the robot picks up an item, the human would drag and guide the arm towards the scanner and have the end-effector hold the item upright for a few seconds before guiding the arm towards the bin. This detour could be simply described as an additional object-centric sub-task, which requires the item to be moved with an upright orientation *relative to* the downward-facing scanner. In this work, we take advantage of this object-centric interpretation of human intentions to enable fast, yet simple online adaptation of robot behaviors.

Existing Approaches: Several approaches have been proposed to adapt robot behaviors using human feedback online. [1] uses human perturbations to infer desired trajectories and incrementally updates learned preferences using maximum posteriori estimation (MAP). [2] assumes that humans intervene based on a linear combination of position and velocity error, and derives an update rule for learned preferences. Although these approaches enable fast, effective adaptation, they assume human preferences are weights for a linear combination of basis functions, such as distance to either a pre-specified object or relative orientation with respect to the goal. However, the linear assumption has limited expressiveness, and the pre-defined basis functions might not cover changing human preferences. This is especially problematic when robots are deployed with new tasks, such as scanning labels under a newly-installed scanner. Our insight is that robots should be able to extract new and flexible preferences from human feedback and leverage them to better adapt future actions.

Our Approach: To address the above challenges, we propose Object Preference Adaptation (OPA) to 1) explicitly

¹Carnegie Mellon University, Pittsburgh, PA. Contact: {ashek, ruic, cliu6}@andrew.cmu.edu

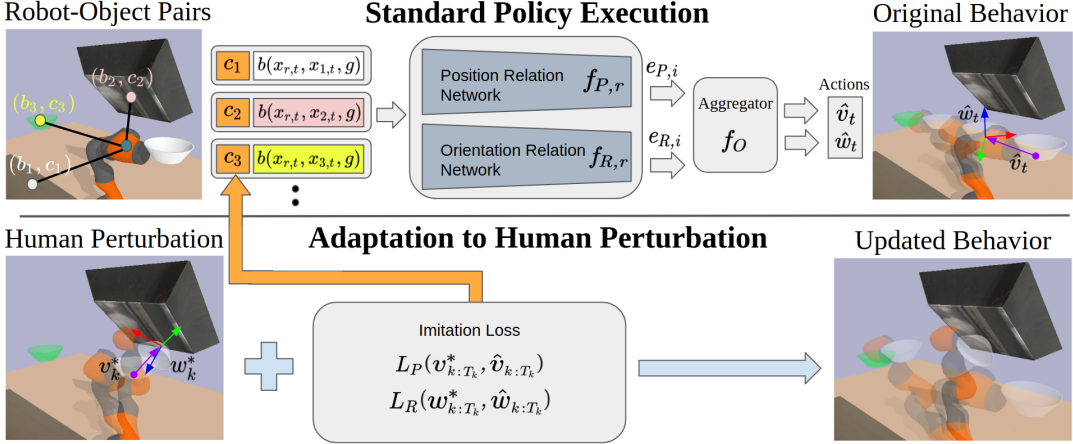


Fig. 2: Illustration of the adaptation with OPA. OPA consists of a position relation network $f_{P,r}$ and an orientation relation network $f_{R,r}$ whose outputs are aggregated by f_O . **Top:** For each object $i \in [N]$ in a scene (including the green goal), a state-based feature $b_R(\mathbf{x}_{r,t}, \mathbf{x}_{i,t}, g)$ is computed from both object state $\mathbf{x}_{i,t}$ and robot state $\mathbf{x}_{r,t}$. This is passed along with a learned, preference feature c_i into each relation network to produce edge features $e_{P,i}$ and $e_{R,i}$. Together, all edge features are fed into an aggregator function f_O that finally computes predicted translation \hat{v}_t shown in purple and orientation \hat{w}_t shown as Cartesian axes in the top right. **Bottom:** In the bottom left, humans can perturb both position and orientation to produce $v_{k:T_k}^*$ and $w_{k:T_k}^*$, which can be treated as ground truth for an imitation loss. Only object preference features c_i are updated, allowing for fast and effective adaptation of behavior such as scanning the bottom of a bowl as shown in the final image to the right.

consider pairwise relations between each object and the robot and 2) interpret human feedback in terms of these relations. We first pre-train a policy to reproduce randomly-generated trajectories that follow a specific pattern: reaching a goal while interacting with nearby objects. The policy parameters are divided into two groups: the core weights encoding the general interaction dynamics between objects, and the object-specific features. We assume there are only four possible classes of object interactions during data generation: either moving closer or farther away in position, and either ignoring or matching the orientation of an object with a fixed rotational offset. Real-world examples of this include moving above and horizontally tilting to pour water into a cup, or staying away from an open flame. As the policy learns to imitate these trajectories, it also learns two key properties: how objects generally influence a trajectory (the interaction dynamics), and how specific types of object relations can be represented in a continuous latent space of finite dimensions.

When adapting to physical perturbations, the core policy weights are frozen because the general dynamics of object interactions should not change. Rather, *object-specific features* need to be adapted to capture various behaviors. In the illustrating example, the scanner should always be able to attract or repel the robot (the dynamics), but which specific behavior and to what extent are object-specific. We argue that such separation can be naturally captured by a graph with the agent and objects as nodes. The interaction dynamics are shared among all edges, while how each node pair influences the robot behaviors also depends on the actual objects. Following this idea, we compose our robot policy based on Graph Neural Network (GNN), which further allows end-to-end learning given human feedbacks. As a result, during online adaptation, we constrain the search to a compact latent space of object-specific features, which can be done with only a few gradient steps. Although our pre-

training data contained only four classes of object relations, optimization over a continuous latent space allows the policy to express new, unseen types of interactions with objects, such as ignoring objects for position, or learning arbitrary 3D orientations relative to an object’s orientation.

To evaluate our model’s adaptability, we invited users to perturb a simulated robot manipulator in three separate tasks. Users would observe the robot’s original behavior, apply perturbations to demonstrate desired behavior, and judge the robot’s updated behaviors. We compare to a baseline which switches to gravity compensation during perturbation, but otherwise tracks the goal in a predefined way. Based on the user study, OPA shows better understanding of human preferences, requires less feedback, and responds to corrections more predictably.

Overall, we summarize our contributions as follows:

- 1) We interpret human physical feedback as object-specific interactions and model these with a graph representation, enabling fast adaptation.
- 2) We show that synthesized data alone can train a policy that handles realistic tasks and unstructured human perturbations.
- 3) We experimentally show impressive adaptability to human perturbation on three challenging tasks.

II. UNDERSTANDING OBJECT-CENTRIC HUMAN FEEDBACK

At time t , let $\mathbf{x}_{r,t} \in \mathbb{R}^d$ represent the current state of the robot r , and $\mathbf{x}_{i,t} \in \mathbb{R}^d$ represent the states of other objects $i \in [N]$ in a scene. This assumes we can detect, uniquely identify, and extract the 6D pose of each object in a scene. We leave unstructured environments for future work.

The robot’s state updates according to dynamics $\mathbf{x}_{r,t+1} = \mathbf{x}_{r,t} + \alpha \mathbf{u}_t$ where α is a constant step size and $\mathbf{u}_t \in \mathbb{R}^{d'}$ is the action either applied externally by the human if

available, or otherwise generated by the policy. We denote the human intervention as \mathbf{u}_t^* and the robot policy as $\hat{\mathbf{u}}_t = f_O(\mathbf{x}_{r,t}, \{\mathbf{x}_{i,t}\}_{i \in [N]}, \mathbf{g})$ where the goal \mathbf{g} is assumed given. The general learning objective is to match the human's actions over T steps:

$$\min_{f_O} \sum_{t \in [T]^*} \|f_O(\mathbf{x}_{r,t}, \{\mathbf{x}_{i,t}\}_{i \in [N]}, \mathbf{g}) - \mathbf{u}_t^*\|, \quad (1)$$

where $[T]^*$ is the set of time indices where human interventions are available.

To infer object-centric meanings from human actions, we represent the scene as a graph, where nodes are the robot and all other objects, and directed edges pointing only from each object to the robot. A graph naturally lets us model each object and its relation to the robot separately; graphs can also capture potential object-centric preferences from human feedback. Note that our approach can be easily extended to consider relations between objects with additional edges. In those cases, our approach shows even more advantage in providing a computationally efficient way to capture complex interactions between objects.

In our graph, each of the agent-object relations is composed of two elements: relative state features $\mathbf{b}_{i,t}$ and learned “preference” features \mathbf{c}_i . State features are computed from robot, object, and goal state $\mathbf{b}_{i,t} = \mathbf{b}(\mathbf{x}_{r,t}, \mathbf{x}_{i,t}, \mathbf{g})$ and help the policy reason about spatial proximity and direction of each object relative to the robot and its goal. Preference features \mathbf{c}_i capture the specific way that each object should interact with the agent. Together, these can be processed by a *relation network* f_r to generate a latent edge features $\mathbf{e}_{i,t} = f_r(\mathbf{b}_{i,t}, \mathbf{c}_{i,t})$, as shown in the top of Fig. 2. We can rewrite the robot’s overall policy as an “aggregator” f_O of edge features $f_O(\{\mathbf{e}_{i,t}\}_{i \in [N]})$ and its objective as

$$\min_{\{\mathbf{c}_i, f_r\}} \sum_{t \in [T]^*} \|f_O(\{\mathbf{e}_{i,t}\}_{i \in [N]}) - \mathbf{u}_t^*\|. \quad (2)$$

Note that we learn preference features \mathbf{c}_i while keeping the manually designed state features $\mathbf{b}_{i,t}$ fixed. This naturally isolates the objective information of the scene from subjective preferences and helps the model to focus on object-specific preference features.

III. OBJECT-CENTRIC REPRESENTATION

We now consider the specific domain of full rigid body motion in 2D or 3D for OPA. Time index t is omitted for clarity. We assume object-specific tasks can generally be represented as reach and avoid, and only focus on this setting without considering the complexity of actual grasping. We leave this for future work. The objects and robot are represented as spheres with radii of influence $s_{i \in [N]}$ and s_r respectively. Tricks to handle non-spherical objects are discussed in task 1 of the experiments.

Actions \mathbf{u} are composed of translation \mathbf{v} and rotation \mathbf{w} actions. \mathbf{v} is a unit vector describing the direction of translation. \mathbf{w} describes the desired orientation at the next timestep. For 2D, $\mathbf{w} = [\cos(\theta), \sin(\theta)]$ for angle θ on the x-y plane. For 3D, $\mathbf{w} = [R_x^T, R_y^T] \in \mathbb{R}^6$ where $R_x, R_y \in \mathbb{R}^3$

are the x and y axes of an orientation expressed by a rotation matrix $R = [R_x, R_y, R_z] \in SO(3)$. This is shown in the top right of Fig. 2, where $\hat{\mathbf{w}}_t$ points from the end-effector’s current to future position, whereas $\hat{\mathbf{w}}_t$ is the future orientation.

States \mathbf{x}_i are separated by position $\mathbf{x}_{P,i}$ and orientation $\mathbf{x}_{R,i}$. State features \mathbf{b}_i are separated by position $\mathbf{b}_{P,i} = \mathbf{b}_P(\mathbf{x}_r, \mathbf{x}_i, \mathbf{g})$ and orientation $\mathbf{b}_{R,i} = \mathbf{b}_R(\mathbf{x}_r, \mathbf{x}_i, \mathbf{g})$. Preference features \mathbf{c}_i are composed of position component $\mathbf{c}_{P,i}$ and orientation component $\mathbf{c}_{R,i}$. $\mathbf{c}_{P,i}$ is purely latent whereas $\mathbf{c}_{R,i} = [\mathbf{c}_{R,i}^{\text{latent}}, \mathbf{c}_{R,i}^{\Delta}]$ is composed of a latent part $\mathbf{c}_{R,i}^{\text{latent}}$ and a learned rotational offset $\mathbf{c}_{R,i}^{\Delta}$. This learned offset is applied directly to the input orientation of an object and allows the model to learn relative orientations. For example, scanning the barcode underneath a bowl in Fig. 2 requires the barcode to face the scanner, and this relative orientation can be represented by a rotational offset.

A. Graph Representation Overview

To process a graph of arbitrarily many object nodes, we choose to use a GNN due to its desirable property of invariance to both the number and ordering of nodes. Also, since GNN’s apply the same network to process every edge in a graph, they enforce a strong inductive bias that general edge computations remain the same. Only each pair of node’s relative features distinguishes specific behavior. This is the key for GNN’s well-known generalization to unseen scenarios.

To process each robot-object node pair, two different networks compute latent edge features: $\mathbf{e}_{P,i} = f_{P,r}(\mathbf{b}_{P,i}, \mathbf{c}_{P,i})$ for position, and $\mathbf{e}_{R,i} = f_{R,r}(\mathbf{b}_{R,i}, \mathbf{c}_{R,i})$ for orientation. Finally, the output actions can be computed using the same function f_O but with different sets of edge features: $\hat{\mathbf{v}} = f_O(\{\mathbf{e}_{P,i}\}_{i \in [N]})$ and $\hat{\mathbf{w}} = f_O(\{\mathbf{e}_{R,i}\}_{i \in [N]})$, as shown in Fig. 2. In the following sections, we will explain the computation of these features for each object and how these are aggregated to produce a single output action.

B. Relation Network and Aggregator

In this section, we first discuss our general relation network f_r used for both position and orientation control, which takes as input pairs of state and preference features $(\mathbf{b}_i, \mathbf{c}_i)$.

Typically, neural network inputs are raw states, hand-crafted state features, or outputs from a separate network. Our approach, however, treats the object-specific features \mathbf{c}_i as updatable weights to be learned with the rest of the network through gradient descent. As our policy trains on the same set of object types, these low-dimensional preference features gradually discriminate to represent very different behaviors. In fact, as will be described in later sections, these object feature spaces can be as small as 1D and still capture diverse behaviors. We note that during training, the object types are provided as input in the form of indices. This enables the model to associate the correct feature \mathbf{c}_i with each object, ensuring that they are trained consistently.

Pairs of state-based and preference features are fed into a multi-layer perceptron (MLP) f_r^1 to produce intermediate

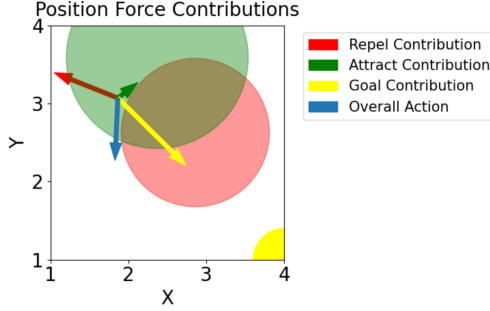


Fig. 3: Position “force” contribution $e_{P,i}$ of each object node along with overall action \hat{v} for a 2D synthetic scene.

features \tilde{e}_i . A second MLP f_r^2 computes unnormalized attention-like weights $\tilde{\alpha}_i$ for these features, and overall edge features $e_i = \tilde{\alpha}_i \tilde{e}_i$ take the form of actual actions. Given this set of weighted actions, the aggregator f_O simply performs a summation followed by a normalization.

For position action \hat{v} , we normalize to a magnitude of 1 to produce a valid unit vector:

$$\hat{v} = \frac{\sum_{i \in [N]} e_{P,i}}{\|\sum_{i \in [N]} e_{P,i}\|} \quad (3)$$

Each object essentially contributes a “force” pushing or pulling on the robot, as shown in Fig. 3.

For orientation \hat{w}_t , we sum up all edge features and normalize for each specific axis:

$$\tilde{w} = \sum_{i \in [N]} e_{R,i} \text{ then } \tilde{w} = \begin{bmatrix} \frac{\tilde{w}_{1:3}}{\|\tilde{w}_{1:3}\|} & \frac{\tilde{w}_{4:6}}{\|\tilde{w}_{4:6}\|} \end{bmatrix}. \quad (4)$$

For the 2D case, $\hat{w} = \tilde{w} \in \mathbb{R}^2$. For the 3D case, however, since our above calculation is essentially a normalized weighted sum of rotation matrices, the resulting $\tilde{w} = [\tilde{R}_x^T, \tilde{R}_y^T]$ is not a valid rotation. \tilde{R}_x and \tilde{R}_y must be orthogonal, and to enforce this, we apply Gram-Schmidt orthogonalization to remove the component of \tilde{R}_y parallel to \tilde{R}_x while keeping $R_x = \tilde{R}_x$:

$$\tilde{R}'_y = \tilde{R}_y - \frac{\langle \tilde{R}_x, \tilde{R}_y \rangle}{\langle \tilde{R}_x, \tilde{R}_x \rangle} \tilde{R}_x \text{ and } R_y = \frac{\tilde{R}'_y}{\|\tilde{R}'_y\|}. \quad (5)$$

The resulting two axes $\hat{w} = [R_x^T, R_y^T]$ alone are sufficient to represent a full rotation in $SO(3)$, where the R_z axis is simply the cross product of the R_x and R_y axes.

C. Position Relation Network

In this section, we describe state-based and preference features for our position relation network. State-based features $b_{P,i}$ are the following:

- 1) **Size-relative distance:** Distance between robot and object divided by the sum of their radii, which helps the policy reason about when to interact with an object.
- 2) **Direction:** Unit-vector pointing from agent to each object, which helps determine the direction of “force” applied on agent.
- 3) **Goal-relative direction:** Inner-product between each agent-object vector and the agent-goal vector. A positive value indicates that the object lies in the same

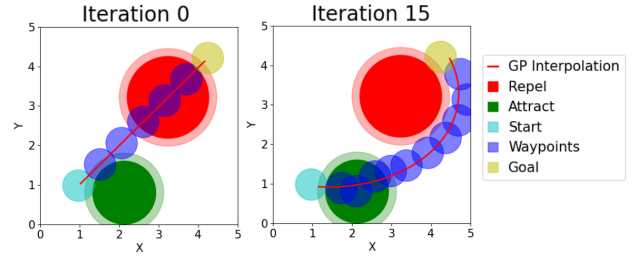


Fig. 4: First and last steps of Elastic Band in 2D. Dark blue agent waypoints traverse from the light-blue start to yellow goal position while interacting with nearby “Attract” and “Repel” objects. A Gaussian Process interpolates between the waypoints.

direction as towards the goal and should be considered.

A negative value indicates the object is “behind” the agent and can be ignored.

Position preference features $c_{P,i}$ intuitively capture the magnitude of the output force, or how attracted or repelled the robot should be from each object. Reducing its dimensionality as much as possible prevents over-fitting while simplifying adaptation in the feature space, and in our experiments, simply using 1D was enough for expressive policy behavior.

The position relation network overall outputs a push-pull force on the agent. Potential field methods [3] also use this approach, but constrain this force vector to be parallel to each agent-object vector. This may seem like an intuitive way to enforce structure in the network and reduce complexity, but this constraint fails during “singularities” where no orthogonal component is available to avoid an obstacle lying in the same direction as the goal.

During training, we measure misalignment between ground-truth v_t^* and predicted \hat{v}_t translation directions using the following loss across B batch samples:

$$L_P = \frac{1}{B} \sum_{b=1}^B 1 - \langle v_b^*, \hat{v}_b \rangle \quad (6)$$

D. Orientation Relation Network

In this section, we describe state-based and learned features for our orientation relation network. State-based features $b_{R,i}$ are the following:

- 1) **Size-relative distance:** identical to that of the position relation network.
- 2) **Modified Orientation:** Orientation of each object, but rotated by a learned rotational offset. This helps the policy output the correct orientation relative to an object’s.

The learned rotational offset $c_{R,i}^\Delta$ is represented as a scalar $\Delta\theta$ for 2D and as a unit-normalized quaternion for 3D. $c_{R,i}^\Delta$ is applied to the x and y axes of the object’s rotation matrix. We choose to manually apply a learned rotational offset to reduce burden on the network of needing to learn how to apply valid rotations. An additional learned feature $c_{R,i}$ intuitively determines whether an object’s orientation should be ignored or not. This is important for modeling real-world

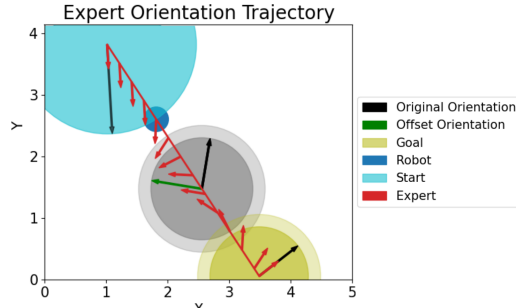


Fig. 5: Example scenario to train the orientation relation network in 2D. Expert path in red is annotated with an orientation vector at each waypoint. Each node (start, grey object, and goal) has both its observed orientation $\mathbf{x}_{R,i}$ shown as a black arrow along with its desired, relative orientation $R(c_{R,i}^{\Delta*}) \cdot \mathbf{x}_{R,i}$ shown in green. The only node with nonzero rotational offset is the grey object: $c_{R,0}^{\Delta*} = -90^\circ$, which is why the green arrows are not visible for start and goal.

tasks where a robot should move closer to an object without changing its orientation, such as handing a glass of water to a person.

Loss can be calculated by measuring the summed misalignment between ground-truth and predicted x and y axes:

$$L_R = \frac{1}{B} \sum_{b=1}^B 2 - \langle R_{x,b}^*, \hat{R}_{x,b} \rangle - \langle R_{y,b}^*, \hat{R}_{y,b} \rangle. \quad (7)$$

IV. TRAINING AND ONLINE ADAPTATION

So far, we have discussed the implementation and intuition behind our policy. We now discuss how to train and adapt such a policy at test time.

A. Training with Synthetic Data

Imitation learning typically requires demonstrations, but collecting human demonstrations can require much effort [4]. However, since our intended real-world tasks can be considered as reaching a goal with midway object interactions, we can generate synthetic data to capture this behavior. For position and orientation specifically, notice how their computation is completely independent. This allows us optimize their losses L_P and L_R separately, bypassing the issue where their units are different and thus require re-weighting [5]. This also allows us to train both networks with different sets of data, which is necessary since the behavior of the position and orientation networks should not be correlated. For example, a trajectory may avoid an obstacle and stay far enough that the obstacle has no influence on the robot's orientation. By training orientation features on this data, the orientation network would learn to just ignore this object's orientation.

For the position network specifically, interactions with nearby objects should take the form of attractions and repulsions; Elastic Bands [6] naturally model this. Fig. 4 shows this process in detail, where the final iteration's trajectory is used to train our position network.

For the orientation network, trajectories involve interactions with a single object of two possible relations: *ignore*

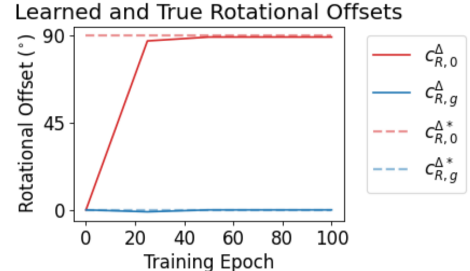


Fig. 6: Comparing the ground truth $c_{R,i}^{\Delta*}$ and learned $c_{R,i}^{\Delta}$ 2D rotational offsets for the considered object $i = 0$ and goal $i = g$ during training. Here, $c_{R,0}^{\Delta*} = 90^\circ$ and $c_{R,g}^{\Delta*} = 0^\circ$.

and *consider*. Ignored objects have no influence on the agent's orientation. Considered objects force the agent to match their original orientation $\mathbf{x}_{R,0}$ relative to an offset $c_{R,0}^{\Delta*}$ shared among all considered objects. Fig. 5 shows an example where the expert orientation of a waypoint must match that of nearby objects. The expert initially matches the start orientation with zero offset, but switches to the grey object's orientation in green with non-zero offset, and finally converges to the goal orientation with zero offset. Our policy would need to predict this relative orientation given only the original black orientation as input.

Since observed orientations $\mathbf{x}_{R,0}$ are randomized while $c_{R,0}^{\Delta*}$ is fixed, our orientation network is forced to properly learn offset $c_{R,0}^{\Delta}$ to predict orientations $R(c_{R,0}^{\Delta*}) \cdot \mathbf{x}_{R,0}$. Fig. 6 compares learned and true rotational offsets during training for the 2D case. The fact that they match shows that carefully chosen model structure can force the learned network weights to be interpretable. Another example in 3D is that, when pouring water from cup A into cup B with upright orientation $\mathbf{x}_{R,B}$, we need to tilt cup A horizontally by $R(c_{R,B}^{\Delta*})$ to match the goal orientation $R(c_{R,B}^{\Delta*}) \cdot \mathbf{x}_{R,B}$.

Our method relies on objects to influence behavior, but we also may desire the robot to fix its orientation throughout a trajectory, even with no objects nearby. A cup of water, for example, should be carried upright. To train this soft constraint, start and goal are treated as imaginary objects whose orientation must also be considered. Both share a true rotational offset of the identity, or zero: $c_{R,g}^{\Delta*} = R(0)$. Fig. 6 visualizes this in blue.

B. Online Adaptation

In this section, we discuss our assumptions on the form of human perturbation as well as how the policy adapts to this to infer human preferences. People think and act differently, and this changes how and when they may intervene in the robot's trajectory. [7] argues that people may intervene only when recent behavior has been unacceptable. This implies that the overall trajectory is not an example of a good trajectory, but rather a *transition* from bad to good. This thus provides information for *how the robot's behavior should change* rather than the absolute trajectory that should be naively imitated.

Following that intuition, we focus only on the human perturbation trajectory $(\mathbf{x}_{k:T_k}^*, \mathbf{u}_{k:T_k}^*)$ and treat this as an

expert trajectory to imitate. A key assumption is that humans only care about the final pose rather than the actual trajectory taken. Based on this assumption, we only take the start and end pose of the perturbation trajectory and linearly interpolate between the two. On the policy side, rather than calculating the output action for each individual expert state $\mathbf{x}_{k:T_k}$, we rollout the policy in an open-loop fashion, starting from initial intervention state \mathbf{x}_k^* and repeatedly taking the policy’s action with deterministic dynamics. This “imagined” rollout makes two assumptions: the physical robot can perfectly track its desired pose, and objects’ poses are fixed or can be predicted. Overall, however, this allows gradients to propagate throughout the entire rollout, and early mistakes will be penalized for future errors. Losses L_P and L_R from (6) and (7) can be calculated and used in standard gradient descent.

However, fine-tuning all weights of a neural network is well-known to lead to inefficient adaptation due to the large number of parameters. We bypass this issue by taking advantage of our graph-based architecture: updating only learned object features $c_{P,i}$ and $c_{R,i}$ while keeping the core relation network weights frozen. This matches our intuition: the general dynamics of interacting with objects should not change. Rather, *only object-specific features* need to be adapted to capture object-specific behaviors. This allows us to drastically change the policy’s behavior with only a few steps of standard gradient descent.

This works surprisingly well, even for the learned rotational offset features $c_{R,i}^\Delta$. Recall that our model only had to learn two rotational offsets: $c_{R,0}^{\Delta*}$ and $c_{R,g}^{\Delta*}$. At test-time, however, our model can quickly adapt to reproduce *any arbitrary rotation* in $SO(3)$.

V. EXPERIMENTS

A. User Study

After pre-training, we evaluated our model’s test-time adaptability to human perturbations. We invited 10 CMU students to participate in three simulated tasks where a robot manipulator’s initial behavior was incorrect. Participants were instructed to press computer keys to perturb the end-effector’s position or orientation at any moment. The current task would either continue or reset to show our model’s updated behavior. The three tasks are shown in Fig. 7. Tasks 1 and 2 evaluate the position and orientation relation networks separately with certain features c_i initialized correctly. Task 3 evaluates both networks together in a more realistic scenario where no prior information about the object is known.

Task 1: Carrying Fragile Cup A robot bartender hands cups of water to customers. Since the cups are fragile, they should be carried low to the table. Participants would push the robot to stay close to and above the table when they felt necessary. The robot would either continue moving straight to the goal (baseline) or perform online adaptation and update its behavior (our model). An example of this updated behavior is shown in Fig. 1. This scene contains three different table objects, and only their position preference features $c_{P,i}$ can be updated. This task highlights our model’s

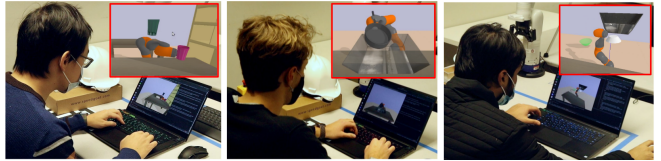


Fig. 7: Experiment tasks 1, 2, and 3 listed from left to right. In task 1, the robot was perturbed as it moved towards the green floating cup representing the goal. In task 2, the user rotated the end-effector to achieve a desired pan orientation above the inspection zone. In task 3, the user perturbed the robot’s position and orientation to demonstrate the additional scanning task before moving to the green goal location.

fast online adaptation. Note that a flat table’s position $\mathbf{x}_{P,i}$ at time t is the orthogonal projection of the end-effector onto its surface.

Task 2: Inspecting Factory Items A robot presents pans to a quality control inspector who wants to view them at different orientations. Participants are shown an image of the pan’s desired orientation and must perturb the robot-held pan to achieve this. Once satisfied, users then reset the episode and judge how closely the robot’s updated orientation matches their final perturbed orientation (not the reference). This challenge involves only updates to the relative rotational offset $c_{R,i}^\Delta$ of the inspection bin, and evaluates the model’s ability to represent arbitrary orientations in $SO(3)$. The linked video visualizes this clearly.

Task 3: Scanning Factory Items A robot initially carries manufactured bowls to a bin. The factory has installed a new barcode scanner, and the robot should midway scan the bottom of each bowl. Participants must perturb both position and orientation, requiring updates to all preference features of the scanner: $c_{P,i}$ for moving closer to it, $c_{R,i}^{\text{latent}}$ for actually caring about its orientation, and $c_{R,i}^\Delta$ for the upside-down orientation relative to it. This task is also shown in Fig 2.

B. Hyper-Parameters

For our experiments, we pre-trained our model using Adam with a learning rate of $lr = 3e-4$ and a batch size of 16 trajectories with 32 random timesteps sampled from each. We synthetically generated 3000 trajectories for both position and orientation datasets, taking 4 minutes each with 9 parallel processes. We trained both position and orientation networks for 100 epochs, taking 12 minutes each on a standard laptop GPU core.

We defined the first MLP’s $f_{P,r}^1$ and $f_{R,r}^1$ of the position and orientation networks as ReLU-activated linear layers with output sizes [64, 64, 64]. The attention-generating MLP’s $f_{P,r}^2$ and $f_{R,r}^2$ had output sizes [16, 8, 1] with activations [ReLU, ReLU, Softmax]. Preference features $c_{P,i}$ and $c_{R,i}^{\text{latent}}$ were only 1-dimensional, whereas rotational offsets $c_{R,i}^\Delta$ were 4-dimensional quaternions.

During online adaptation, we fine-tuned our object features with Adam and a learning rate of $lr = 0.1$, and specifically ran 5 gradient updates for the position network and 20 for the orientation network, taking less than 0.5 seconds in total.

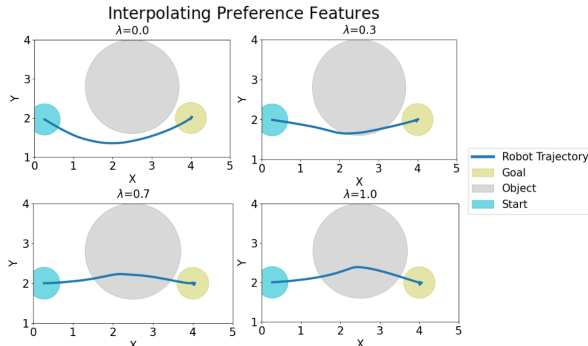


Fig. 8: Resulting change in robot’s behavior as the grey object’s preference feature shifts between “repel” $c_{P,0}$ and “attract” $c_{P,1}$ according to $(1 - \lambda)c_{P,0} + \lambda c_{P,1}$.

C. Feature Initialization

Optimizing deep neural networks is notoriously non-convex, so weight initialization is important to consider. During training, we specifically initialize position preference features $c_{P,i}$ of repulsion, attractor, and goal object as [1.0, 0.5, 0.0]. This prior tries to ensure that at the end of training, interpolating from one feature to another leads to interpolation in behavior space. This interpolation allows us to reasonably guess the feature value representing “ignore” behavior, which is how any new, unseen object should be initially treated. We visualize the interpolation in Fig. 8. As c_P of the grey object interpolates from learned “repel” $c_{P,0}$ to “attract” $c_{P,1}$, the robot clearly moves closer to the object. The indices 0 and 1 refer to an arbitrary repel object and an arbitrary attract object respectively. At test-time, any new objects can be approximately initialized as “ignore” with value $(c_{P,0} + c_{P,1})/2$.

D. Results

Now that we have explained the model implementation details used in our experiments, we discuss the results. After participants finished each task, they would fill out an anonymous survey to provide feedback with answers either descriptive or on a five-point scale.

Task 1:

- 1) Did they think the robot understood their intentions?
- 2) Did they exert a lot of effort to correct the robot?
- 3) Did the robot’s reactions to their pushes match their expectation?
- 4) How satisfied were they about the robot’s behavior?
- 5) Number of user interventions
- 6) Average distance of cup to table.

Figure 9 shows users felt our model understood their preferences better, required less effort, and were slightly more predictable after perturbations when compared to the baseline. Note that users were not told which system (baseline or our model) was being tested. Users generally felt that our model understood the “underlying objective of keeping the glass closer to the table”. Two users noted that our model was sometimes unpredictable, lingering near the table too long and even ignoring the goal completely. This raises an important issue with over-fitting to short human perturbations and

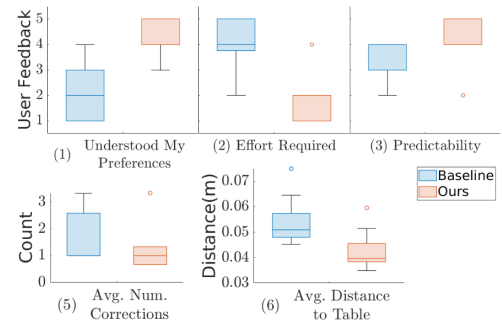


Fig. 9: Task 1 user feedback for both baseline and our model, where each box plot is numbered according to the original list of Task 1 questions.

highlights our model’s sensitivity to the hyper-parameters of adaptation learning rate and number of steps.

Task 2:

- 1) Did the robot present items how they wanted?
- 2) Error between robot and user’s final perturbed orientation.

The 1st quartile, median, and 3rd quartile values for question one were 3.5, 4.0, and 4.0 respectively. For question two, we define orientation error between two quaternions q_1, q_2 as $\text{arccos}(|q_1 \cdot q_2|) \in [0, \frac{\pi}{2}]$ [8]. Average error was 0.2576, or 16% of the max possible error $\frac{\pi}{2} = 1.5708$. This indicates that our model matched users’ desired orientations well.

Task 3:

- 1) Did they think the robot understood their intentions?
- 2) How satisfied were they about the robot’s behavior?

The 1st quartile, median, and 3rd quartile values for question one were 4.0, 4.0, and 5.0 respectively, indicating that users were very satisfied with our model’s adaptability. This sentiment was also generally present in the second question. However, two users noted that the bowl should have moved closer to the scanner. This indicates that more gradient steps were needed, and again highlights the difficulty of tuning such parameters. A practical way to ensure the robot converges to an object is to simply treat it as a goal itself and define any complex task as a sequence of sub-goals.

VI. RELATED WORK

A. Online Adaptation from pHRI

Inverse Reinforcement Learning (IRL) methods attempt to model the preferences θ of an agent by observing its behavior [9]. The agent’s actions presumably maximize a reward function parameterized by θ , and the goal is that inferring correct θ will help model the agent’s behavior. Observations are often limited and noisy, which creates much ambiguity: many reward functions could represent these demonstrations [10].

IRL methods often address this by constraining the space of rewards to be composed of pre-specified basis functions $\phi(x)$ with unknown weights θ : $r(x) = \theta^T \phi(x)$. Existing methods handle noise [10], passively observe demonstrations [11], or even update online from corrections [1], [2]. This allows for fast adaptation and expressive trajectories, but strongly assumes that the *fixed set of functions* $\phi(x)$ can

sufficiently capture the intentions of humans. However, this assumption often will not hold when tasks are modified or executed in new environments. [12], [13] can generate new reward basis functions, but require multiple expert demonstrations and thus do not handle online feedback. Our method dynamically varies its reward functions as objects leave or enter a scene, where such functions are online optimized in continuous latent space using human feedback.

B. Object-Centric Manipulation Policies

The idea of representing the world as a graph of object-based nodes has been applied to modeling particle physics [14], [15], complex robot dynamics [16], and even visual scenes [17]. Existing methods also apply this to visually imitate demonstrations [18] and hierarchically compose object-centric controllers [19]. Graphs can decompose complex dynamics and behaviors into a collection of simpler, object-object interactions. This has served as important inductive bias for helping Graph Neural Networks (GNN) generalize beyond training data [20]. We extend this idea to IRL and the challenge of understanding human preferences from unstructured, physical perturbations.

C. System Identification and Adaptation

Our method pre-trains a base policy and only adapts object-specific features at test-time to dramatically change behavior. This is similar to methods that condition a policy on real physics parameters [21] or latent embeddings [22]. Rather than estimating the parameters of the world [22], we estimate the object preferences of a human. Since we have some form of supervision through human perturbations, our latent features can be adapted using standard gradient descent as opposed to learning an explicit adaptor network [22]. By separating latent features by object, our latent feature space is much more compact and easier to optimize over.

VII. CONCLUSION

We presented Object Preference Adaptation (OPA), a method for inferring human intentions for objects from physical corrections. OPA represents the environment as a graph with nodes as objects and edges between each object and the agent. Our method was able to fine-tune wrong behavior and learn new complex tasks in our experiments, all from a few physical perturbations. After pre-training an expressive base policy, OPA only needs to optimize object-specific features in a compact latent space, allowing for fast, effective adaptation. Robots and really any deep learning model must be flexible to ever-changing tasks and environments; we believe the key is to separate fixed, fundamental dynamics from task, environment, or object-specific behavior.

OPA relies heavily on object-centric actions and frames tasks as reach and avoid. Many tasks, however, also require fine-tuned grasping and even application of force (ie: wiping a surface). It would be exciting to extend this approach to also handle these complex behaviors. Tasks are not always object-relative but can be task-centric, such as drawing; the combination of both paradigms would be exciting.

ACKNOWLEDGEMENT

We would like to thank Letian Wang and Weiye Zhao for their useful feedback.

REFERENCES

- [1] A. Bajcsy, D. P. Losey, M. K. O’Malley, and A. D. Dragan, “Learning robot objectives from physical human interaction,” in *Proceedings of the 1st Annual Conference on Robot Learning*, ser. Proceedings of Machine Learning Research, S. Levine, V. Vanhoucke, and K. Goldberg, Eds., vol. 78. PMLR, 13–15 Nov 2017, pp. 217–226.
- [2] D. P. Losey and M. K. O’Malley, “Learning the correct robot trajectory in real-time from physical human interactions,” *J. Hum.-Robot Interact.*, vol. 9, no. 1, Dec. 2019.
- [3] J.-C. Latombe, *Potential Field Methods*. Boston, MA: Springer US, 1991, pp. 295–355.
- [4] A. Mandlekar, J. Booher, M. Spero, A. Tung, A. Gupta, Y. Zhu, A. Garg, S. Savarese, and L. Fei-Fei, “Scaling robot supervision to hundreds of hours with roboturk: Robotic manipulation dataset through human reasoning and dexterity,” in *2019 IEEE/RSJ International Conference on Intelligent Robots and Systems (IROS)*. IEEE, 2019, pp. 1048–1055.
- [5] R. Groenendijk, S. Karaoglu, T. Gevers, and T. Mensink, “Multi-loss weighting with coefficient of variations,” 2020.
- [6] S. Quinlan and O. Khatib, “Elastic bands: connecting path planning and control,” in *[1993] Proceedings IEEE International Conference on Robotics and Automation*, 1993, pp. 802–807 vol.2.
- [7] J. Spencer, S. Choudhury, M. Barnes, M. Schmitte, M. Chiang, P. Ramadge, and S. Srinivasa, “Learning from interventions: Human-robot interaction as both explicit and implicit feedback,” 07 2020.
- [8] D. Huynh, “Metrics for 3d rotations: Comparison and analysis,” *Journal of Mathematical Imaging and Vision*, vol. 35, pp. 155–164, 10 2009.
- [9] S. Arora and P. Doshi, “A survey of inverse reinforcement learning: Challenges, methods and progress,” 2020.
- [10] B. D. Ziebart, A. Maas, J. A. Bagnell, and A. K. Dey, “Maximum entropy inverse reinforcement learning,” pp. 1433–1438, 2008.
- [11] A. Y. Ng and S. J. Russell, “Algorithms for inverse reinforcement learning,” in *Proceedings of the Seventeenth International Conference on Machine Learning*, ser. ICML ’00. San Francisco, CA, USA: Morgan Kaufmann Publishers Inc., 2000, p. 663–670.
- [12] A. Bobu, M. Wiggert, C. Tomlin, and A. D. Dragan, “Feature expansive reward learning,” *Proceedings of the 2021 ACM/IEEE International Conference on Human-Robot Interaction*, Mar 2021.
- [13] S. Levine, Z. Popovic, and V. Koltun, “Feature construction for inverse reinforcement learning,” in *Advances in Neural Information Processing Systems*, J. Lafferty, C. Williams, J. Shawe-Taylor, R. Zemel, and A. Culotta, Eds., vol. 23. Curran Associates, Inc., 2010.
- [14] P. W. Battaglia, R. Pascanu, M. Lai, D. Rezende, and K. Kavukcuoglu, “Interaction networks for learning about objects, relations and physics,” 2016.
- [15] A. Sanchez-Gonzalez, J. Godwin, T. Pfaff, R. Ying, J. Leskovec, and P. W. Battaglia, “Learning to simulate complex physics with graph networks,” 2020.
- [16] A. Sanchez-Gonzalez, N. Heess, J. T. Springenberg, J. Merel, M. Riedmiller, R. Hadsell, and P. Battaglia, “Graph networks as learnable physics engines for inference and control,” 2018.
- [17] A. Agarwal, A. Mangal, and Vipul, “Visual relationship detection using scene graphs: A survey,” 2020.
- [18] M. Sieb, Z. Xian, A. Huang, O. Kroemer, and K. Fragkiadaki, “Graph-structured visual imitation,” 2020.
- [19] M. Sharma, J. Liang, J. Zhao, A. LaGrassa, and O. Kroemer, “Learning to compose hierarchical object-centric controllers for robotic manipulation,” 2020.
- [20] P. W. Battaglia, J. B. Hamrick, V. Bapst, A. Sanchez-Gonzalez, V. Zambaldi, M. Malinowski, A. Tacchetti, D. Raposo, A. Santoro, R. Faulkner, C. Gulcehre, F. Song, A. Ballard, J. Gilmer, G. Dahl, A. Vaswani, K. Allen, C. Nash, V. Langston, C. Dyer, N. Heess, D. Wierstra, P. Kohli, M. Botvinick, O. Vinyals, Y. Li, and R. Pascanu, “Relational inductive biases, deep learning, and graph networks,” 2018.
- [21] W. Yu, J. Tan, C. K. Liu, and G. Turk, “Preparing for the unknown: Learning a universal policy with online system identification,” 2017.
- [22] A. Kumar, Z. Fu, D. Pathak, and J. Malik, “Rma: Rapid motor adaptation for legged robots,” 2021.